ACS OMEGA

http://pubs.acs.org/journal/acsodf

Article

Mechanical and Biocompatibility Properties of Sintered Titanium Powder for Mimetic 3D-Printed Bone Scaffolds

Sanghyeon Choi, Ji-Woong Kim, Seungtaek Lee, Woo Young Yoon,* Yuna Han, Ki-Joo Kim, Jong-Won Rhie, Tae-Suk Suh, and Kyung-Don Lee

Cite This: *ACS Omega* 2022, 7, 10340−10346

Read Online

ACCESS | Metrics & More | Article Recommendations | Supporting Information

ABSTRACT: A composite comprising Ti and NaCl powders was sintered similar to a three-dimensional (3D)-printed patient-customized artificial bone scaffold. Additionally, a proper microstructure of the mimetic scaffold and the optimum processing parameters for its development were analyzed. The mechanical properties of the metal-based porous-structured framework used as an artificial bone scaffold were an optimum replacement for the human bone. Thus, it was confirmed that patient-customized scaffolds could be manufactured via 3D printing. The 3D-printed mimetic specimens were fabricated by a powder-sintering method using Ti for the metal parts, NaCl as the pore former, and polylactic acid as the biodegradable binder. Scanning electron microscopy (SEM) images showed that pores were formed homogeneously, while X-ray computed tomography confirmed that open pores were generated. The porosity and pore size distribution were measured using a mercury porosimeter, while the flexural strength and flexural elastic modulus were calculated using the three-point bending test. Based on these measurements, a pore-former content of 15 vol % optimized the density and flexural strength to 2.52 g cm^{-2} and 283 MPa, respectively, similar to those of the actual iliac bone. According to the 3D-printing production method, a selective laser-sintering process was applied for the fabrication of the mimetic specimen, and it was determined that the microstructure and properties similar to those of previous metal specimens could be achieved in the as-prepared specimen. Additionally, a decellularized extracellular matrix (dECM) was used to coat the surfaces and interiors of the specimens for evaluating their biocompatibilities. SEM image analysis indicated that the adipose-derived stem cells grew evenly inside the pores of the coated specimens, as compared with the bulky Ti specimens without the dECM coating. The doubling time at 65% was measured at 72, 75, and 83 h for specimens with pore-former contents of 5, 10, and 15 vol %, respectively. The doubling time without the pore former was 116 h. As compared with the specimens without the pore former (73 h), 15% of the dECM-coated specimens showed a doubling time of 64%, measured at 47 h.

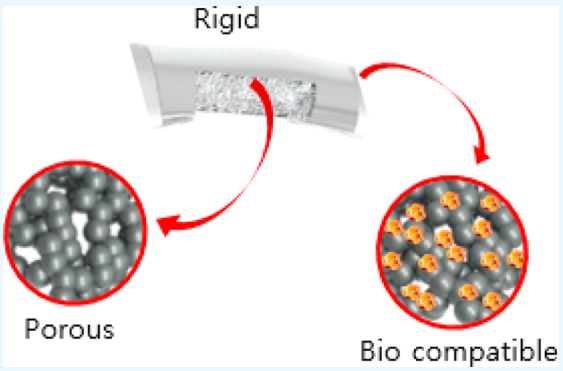

1. INTRODUCTION

There has been an increasing demand for three-dimensional (3D)-printed patient-customized artificial bone scaffolds for the replacement of bone structures due to bone loss;[1,2] however, a proper scaffold microstructure and the optimum processing parameters have not yet been completely realized. Currently, artificial bone scaffolds used in practical applications are primarily fabricated from ceramic materials because their chemical composition is similar to that of real bones.[3,4] However, ceramic materials have mechanical and formability-related disadvantages and are biologically unstable and incompatible.[5,6] Hence, the development of a metal-based bone scaffold without these problems requires further investigation.

Nickel, cobalt, zirconium, aluminum, titanium, and their alloys are currently being used in the fabrication of metallic artificial bone scaffolds.[7] Among them, Ti is considered the most prominent material because of its biocompatibility and excellent weight-to-strength ratio.[8−10]

In terms of manufacturing patient-customized artificial bone scaffolds, it is important to identify a suitable fabrication method based on the shape, strength, and density of the bones, defects, and patient requirements. The most widely used method for molding metals is the casting method.[11,12]

The casting method is inexpensive and allows easy fabrication; however, molded metal exhibits a microstructure that is too compact to build bone scaffolds. Compactly constructed bone scaffolds are too dense and exhibit

Received: December 9, 2021
Accepted: February 25, 2022
Published: March 16, 2022

https://doi.org/10.1021/acsomega.1c06974
ACS Omega 2022, 7, 10340−10346

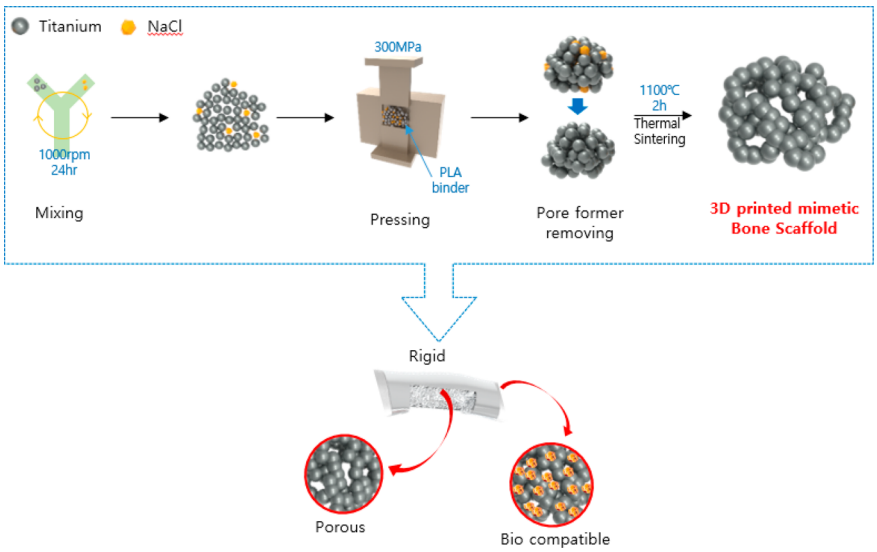

Figure 1. Schematic of the steps in the experimental procedure.

mechanical strengths greater than those of actual bones.[13] As a result, when inserted into the body, such metal scaffolds are incompatible with the surrounding bones because of the differences in their physical properties, thus resulting in stress shielding and implant loosening at the interface.[14−16]

To compensate for these shortcomings, various methods to secure pores in the scaffold microstructure have been employed, as demonstrated in previous studies, for modulating the properties of the scaffold.[17−19] Fujibayashi et al.[20] conducted a study on controlling the density through the formation of a Ti foam structure. They also conducted a study on the production of a bioactive Ti structure by controlling the density and strength of porous Ti blocks and Ti fiber-mesh cylinders using NaOH as the pore former. Using the methods reported in previous papers, we found that it was easy to control the physical properties of the scaffold by securing a large pore. However, an artificial bone scaffold should ideally exhibit fine pores with a controllable pore distribution.[21,22] In addition, smaller artificial bone scaffolds pose limitations to the possible detailing of the fabrication process. Another disadvantage is that bone scaffolds must be produced individually, and it is inconvenient and time-consuming to mold individual shapes for customized fabrications.

Metal 3D printing can optimally control the pore size and distribution for the production of an appropriate bone scaffold.[23] In particular, 3D-printing methods using selective laser sintering can be applied to correct the defect by adjusting the output and speed of the laser source.[24] Although 3D printing is well suited for the production of fine patient-specific artificial bone scaffolds in a single process, various types of specimens must be manufactured under various conditions to understand the microstructure and physical characteristics of the artificial bone scaffold. Therefore, in this study, specimens similar to 3D-printed specimens were fabricated. Experiments using 3D-printed mimetic specimens obtained through the powder-sintering method were conducted, which allowed easy modification of the process conditions and were inexpensive, and shortened the processing time.[25,26]

Using mimetic 3D-printed specimens prepared using the powder-sintering method, we investigated the density and strength of the bone scaffold. These specimens were fabricated using sodium chloride as the pore former, which could be easily eliminated to produce specimens with various porosities.

Spotted as a promising bio ink decellularized extracellular matrix (dECM) are used as cell proliferation agent. The most important function of dECM is structural support for tissue and organ morphogenesis. In addition, it can be also improving cell proliferation and tissue regeneration in artificial bone scaffolds.[27−29]

Moreover, multiple protein adhesion domains of the dECM can localize and present soluble growth factors. In addition, tissue-specific ECMs extend distinct chemical signals into surrounding cells, triggering distinct cellular responses. A more detailed explanation and contents on dECM can be found in the review paper researched by Cho et al.[30]

The internal and external surfaces of an open-pored Ti scaffold were coated with dECM to conduct cell-proliferation experiments. We found that the biocompatibility of the scaffold was secured by improving cell proliferation and tissue regeneration around the scaffold.

In this study, mimetic 3D-printed artificial bone scaffold specimens with various densities and strengths were fabricated to test the suitability of 3D printing for the production of patient-specific bone scaffolds. In addition, we produced a biocompatible artificial bone scaffold by coating the scaffold with dECM bioink.

2. MATERIAL AND EXPERIMENTS

To verify the suitability of 3D printing for the production of biomimetic specimens, the physical properties and microstructures of the mimetic 3D-printed specimens were compared with those of actual 3D-printed metal specimens. Figure 1 shows a schematic of the experimental procedure used in the present research.

Ti powder with particle sizes ranging from 50 to 100 μm and six types of three-base NaCl (0%, 10%, and 15% by volume and 100 μm, 100−200 μm, and 200 μm of size) as the pore former were mixed and stirred well for 24 h at 1000 rpm in a Y-shaped tube. The mixture was subsequently placed in a cemented carbide mold (9 × 35 mm). Thereafter, 3 g of polylactic acid (PLA, MakerBot flexible filament) was dissolved in acetone (30 mL), and 0.6 mL of the mixture was placed in

https://doi.org/10.1021/acsomega.1c06974
ACS Omega 2022, 7, 10340−10346

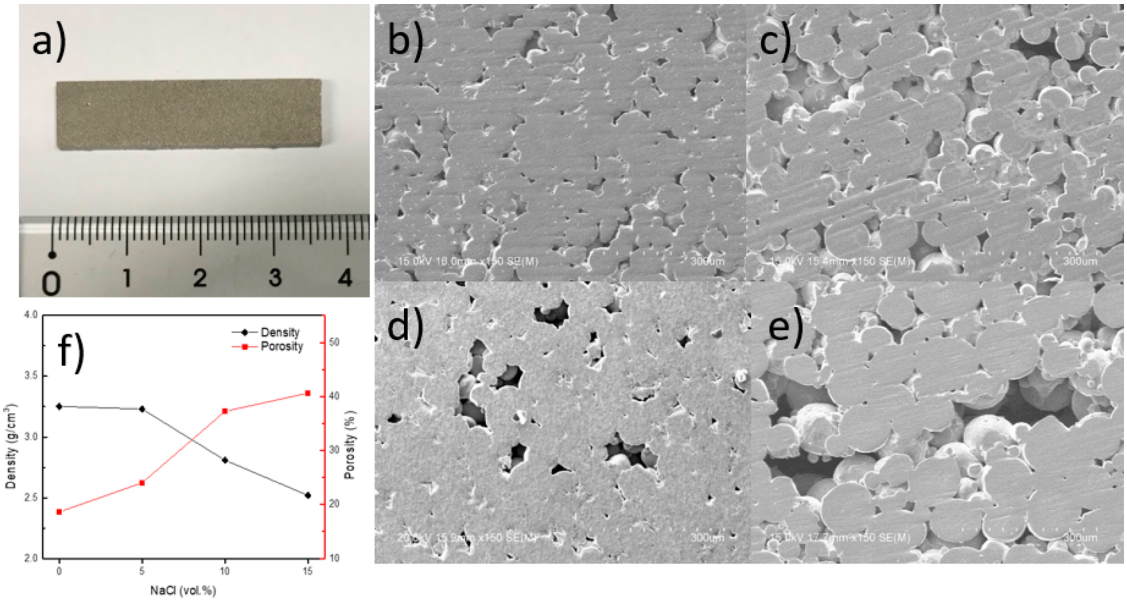

Figure 2. (a) Photograph of the porous Ti scaffold used for the three-point bending test; SEM images of Ti scaffold with (b) 0 vol % pore former, (c) 5 vol % pore former, (d) 10 vol % pore former, and (e) 15 vol % pore former. (f) Porosity and density versus the quantity of the pore former.

the mold and allowed to disperse for 5 min. After 10 min of compression at 300 MPa using a compressor, the NaCl was removed and placed in deionized water for 1 d. Postdrying, the prepared specimens were processed via sintering in a horizontal furnace for 2 h at 1100 °C and a heating rate of 5 °C min^{-1}.

Prior to 3D printing, the 3D modeling tool "Meta Sequoia" was used to model a pellet shape (9 × 35 × 3 mm) suitable for the three-point bending test. Thereafter, two types of Ti-pellet specimens, with porosities of 0% and 27%, were manufactured using a metal 3D printing machine (ORLAS Creator RA).

The porosity and density of the fabricated specimens were measured via mercury porosimetry (Quantachrome, PM33GT). Thereafter, the surface was analyzed using scanning electron microscopy (SEM) (Su-70) and X-ray computed tomography (CT) for determining the pore distribution and internal structure, respectively.

The breaking strengths of the fabricated specimens were measured for a span length of 25 mm and at a moving speed of 1 mm min^{-1} in the three-point flexural mode of a universal testing machine (UTM). The compressive yield strengths of the compressive specimens were measured at a moving speed of 1 mm min^{-1} in compressive mode. Thereafter, the breaking and compressive strengths were measured using an MTDI analysis program (Data analysis ver. 2.43).

All scaffolds were coated with dECM bioink (T&R Biofab Co. Ltd., Seoul, Korea). The dECM bioink solution was prepared using bone bioink, and the component (acetic acid) was mixed for pH adjustment. The scaffolds were coated via centrifugation at 2500 rpm and 4 °C for 3 min. The coated scaffolds were incubated at 37 °C for 45 min for gelation and subsequently freeze-dried. Adipose-derived stem cells (ADSCs), at a density of 7000 cells cm^{-2}, were seeded into the scaffold. The doubling time was measured for each dECM-coated and uncoated specimen using the Cell Counting Kit-8 (CCK-8, Dojin Laboratories, Kumamoto, Japan). The use of ADSCs for this study was approved by Seoul St. Mary's Hospital of Korea (KCMC06BR067).

3. RESULTS AND DISCUSSION

A Ti sample was fabricated (9 × 35 × 3 mm) for the three-point bending test, as shown in Figure 2a. The SEM images of the specimens prepared with different volume percentages of the pore former (0, 5, 10, and 15 vol %) are shown in Figure 2b–e, respectively. As the amount of pore former increased, the number of pores inside the specimen increased, confirming that NaCl acted as the pore former. In addition, after observing the network of the Ti powder structure, we confirmed that the specimen produced by the compression sintering process retained its shape.

Figure 2f shows the porosity and density graph for the various pore former contents, indicating that the porosity of the specimen increased with increasing pore-former content. In the case of Ti-0% (without pore formers), the specimen exhibited 19% porosity, which is characteristic of a powder specimen, caused by the formation of fine pores with sizes <10 μm between the powder particles. As the porosity increased, the density of the specimen decreased. For Ti-15%, the actual cortical density (2 g cm^{-3})[31] of the specimen was approximately 2.52 g cm^{-3}, thus indicating that the Ti-15% specimen was the most biocompatible.

The density, porosity, and physical strength were measured by a mercury porosimeter, and the results of the three-point bending test for the specimen were compared numerically with those for the natural iliac bone (Table 1). It was confirmed that the microstructure and physical strength of the specimen were similar to those of the iliac bone.

Figure 3 shows the flexural strength and elastic modulus of the Ti specimens in the three-point bending test. The flexural strength of Ti-0% (pure Ti specimen) (445 MPa) was higher than that of the real bone (100 to 200 MPa). The specimen appeared superior in strength; however, when there is a large difference in the physical strength at the interface between the artificial bone scaffold and natural human long bone, stress shielding occurred, and the strength of the contacted long bone gradually weakened. Conversely, the Ti-15% specimen demonstrated a flexural strength of 283 MPa and elastic

https://doi.org/10.1021/acsomega.1c06974
ACS Omega 2022, 7, 10340−10346

Table 1. Mechanical Properties of the Ti Scaffolds Depending on the Pore Former Fraction

NaCl (vol %)	density (g cm^{-3})	porosity (%)	flexural strength (MPa)	flexural elastic modulus (GPa)
0	3.25	19.0	445	50
5	3.23	24.0	362	40
10	2.81	37.3	291	38
15	2.52	40.6	283	32
bone	~2	–	103–238	17–23
bulk Ti	4.51	–	200–1000	100–110

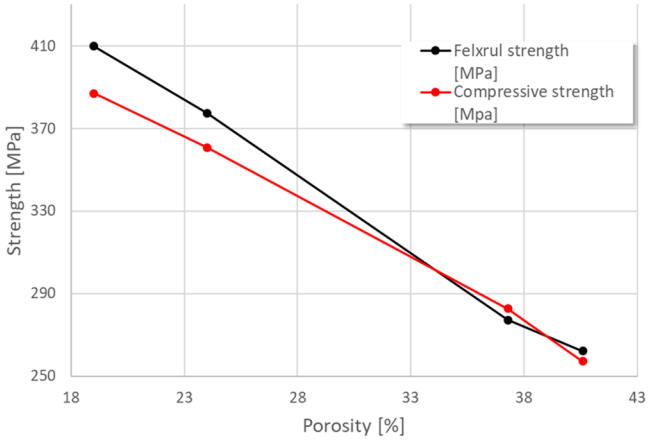

Figure 3. Mechanical strength relative to the porosity of the specimens.

modulus comparable to those of the actual long bone, thus indicating that the Ti-15% specimen exhibited compatible mechanical properties.[32] Furthermore, the results of the compressive test were similar to those of flexural strength test, as shown in Figure 3. These findings indicate that the artificial bone scaffold was able to withstand impacts regardless of the direction of the applied stress. Accordingly, a study of the parameters associated with 3D-printed specimens containing 15% NaCl will be conducted in the future.

To ensure the validity of the mimetic 3D-printed specimens, the physical properties of the specimens fabricated by selective laser sintering (SLS) using the 3D printer ORLAS Creator RA and the mimetic 3D-printed specimens obtained by compression sintering were compared. After the process conditions were set to secure a porosity similar to that of the compression-sintered specimen, the SLS metal 3D-printed specimen was produced and compared with the compression-sintered specimen (Figures S1 and S2). The 3D-printing process carried out under various conditions will be reported in a future study.

Notwithstanding that sufficient similarity to the iliac bone was achieved by adjusting the density and strength of the specimen, additional processing steps were necessary to achieve biocompatibility in the artificial bone scaffold in this study. As such, the specimens were coated with dECM, which was also used for 3D printing, both on the internal and external surfaces of the Ti bone scaffold.

We initially secured the pore size for cell proliferation.[33,34] Figure 4a–c shows the adjusted pore sizes of the pore former (100 μm, 100–200 μm, and 200 μm, respectively), and pore sizes ranging from 100 to 200 μm were found to be the most advantageous for cell proliferation according to the microstructures observed in the SEM results. However, for

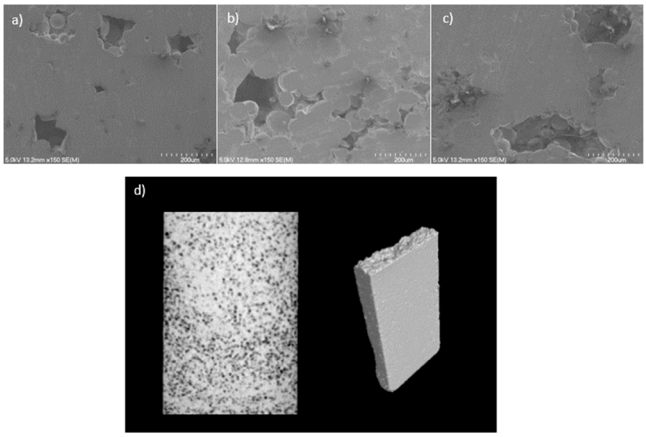

Figure 4. SEM images of the Ti scaffold, depending on the size of the pores: (a) approximately 100 μm, (b) 100–200 μm, and (c) approximately 200 μm. (d) X-ray CT image of the 15 vol % 100–200 μm Ti scaffold.

specimens with a pore size of 200 μm, a pore size of 300 μm was likewise produced. Thus, we determined that the specimens produced with pore sizes ranging from 100 to 200 μm were the most suitable for building the bone scaffold.

For the dECM bioink, to evenly coat the interior surface of the Ti scaffold, a network of pores must be formed.[35] To confirm this, X-ray CT of the Ti-15% specimen with pore sizes ranging from 100 to 200 μm was carried out. The results showed that the pores were homogeneous and that the open pores were well-formed (Figure 4d).

The multilineage differentiation of dECM was excellent; hence, it was possible to secure a certain level of biocompatibility regardless of the part of the body to which the scaffold was applied. According to Cho et al.,[36] an animal-bone-derived stem cell, which induced MSCs on the treated surface, facilitated cell growth and thus exhibited desirable results. This was found to improve osteogenesis of the scaffold.[37]

In addition, the dECM bioink was evenly coated on the scaffold surface and pores.[38−40] As shown in Figure 5, the dECM was coated on the surface, in the pores, and inside the scaffold. As a result of ADSC proliferation in the dECM-coated

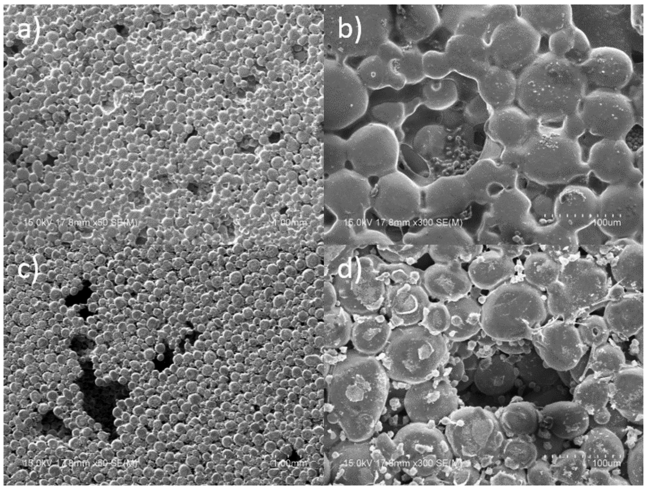

Figure 5. SEM images of (a, b) Ti scaffold coated with dECM and (c, d) cell cultures on the dECM-coated Ti scaffold.

https://doi.org/10.1021/acsomega.1c06974
ACS Omega 2022, 7, 10340−10346

scaffold, the cells grew inside the scaffold, thus obtaining pores with a size suitable for cell growth.

The cell-doubling times based on the pore-former contents were measured for the dECM-coated and uncoated specimens (Figure 6). The uncoated specimens with no pore former (0 vol %) demonstrated a doubling time of 116 h, as compared with 72, 75, and 83 h for the specimens with pore formers (5, 10, and 15 vol %, respectively). Therefore, macropores were found to affect cell proliferation. However, it was difficult to compare the significant differences obtained owing to the amount of pore former that was used. For the dECM-coated specimens, differences due to the pore size were easily observed. The doubling times were 88, 50, 47 h for 5, 10, 15 vol % pore-former contents, respectively. It was confirmed that 15% of the specimens, as compared with the specimens without voids, exhibited a doubling time of 65% regardless of the coating. Thus, it can be observed that cell proliferation can be increased by increasing the surface area of the scaffold, where cells grow due to the macropores generated upon the addition of the pore former.

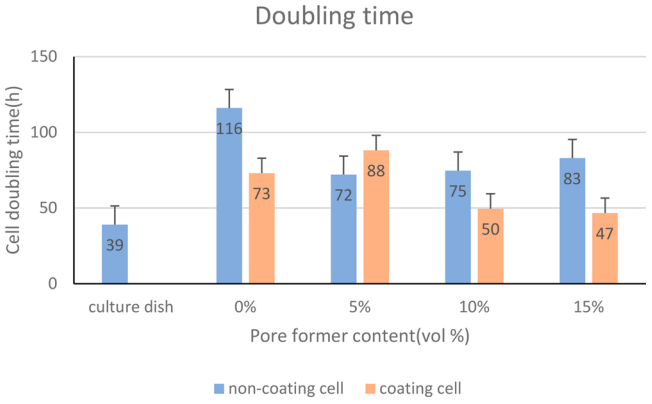

Figure 6. Doubling time of ADSCs, according to the pore former content.

Further research is necessary with respect to the development of patient-specific artificial bone scaffolds via 3D printing along with the database obtained in this study. Furthermore, research on the use of stainless steel, which is inexpensive, is likewise important.

4. CONCLUSIONS

In this study, to apply the 3D-printing method, which is suitable for the fabrication of patient-specific scaffolds, a mimetic 3D-printed Ti scaffold was fabricated, and its mechanical properties and microstructure were investigated. The porosity of the scaffold was controlled by adjusting the amount of NaCl used as the pore former, which could readily be eliminated. Thereafter, experiments were performed, which determined that a specimen obtained using 15 vol % pore former achieved a density of 2.52 g cm^{-3} similar to that of natural human long bone. In addition, the optimum conditions for fabrication, indicated by a similar specimen strength of 283 MPa, were achieved. Additionally, cell-proliferation experiments were conducted by coating the surface of the fabricated scaffold with dECM, a type of bioink. In both the dECM-coated and uncoated specimens, the pore former exhibited an approximately 65% doubling time, thus indicating that macropores affected the cell-proliferation capacity. Through this study, it was possible to understand the properties of the materials required for the fabrication of a Ti scaffold via 3D printing. Furthermore, other biocompatible metals, such as stainless steel 316L, can be used with this method in future studies.

■ ASSOCIATED CONTENT

Supporting Information

The Supporting Information is available free of charge at https://pubs.acs.org/doi/10.1021/acsomega.1c06974.

Figure S1: SEM images of press sintering specimens and 3D printing specimens (a, b) press sintering specimen, (c, d) 3-D printed specimen. Figure S2: Comparison table of density, porosity and mechanical strength of press sintering specimens and 3D printing specimens (PDF)

■ AUTHOR INFORMATION

Corresponding Author

Woo Young Yoon − *Department of Materials Science and Engineering, Korea University, Seoul 136-701, Republic of Korea;* orcid.org/0000-0002-8482-9769; Email: wyyoon@korea.ac.kr

Authors

Sanghyeon Choi − *Department of Materials Science and Engineering, Korea University, Seoul 136-701, Republic of Korea*

Ji-Woong Kim − *Department of Materials Science and Engineering, Korea University, Seoul 136-701, Republic of Korea*

Seungtaek Lee − *Department of Materials Science and Engineering, Korea University, Seoul 136-701, Republic of Korea*

Yuna Han − *Department of Biomedicine and Health Sciences, College of Medicine, The Catholic University of Korea, Seoul 03083, Republic of Korea; Department of Plastic and Reconstructive Surgery, Seoul St. Mary's Hospital, College of Medicine, The Catholic University of Korea, Seoul 06591, Republic of Korea*

Ki-Joo Kim − *Department of Plastic and Reconstructive Surgery, Seoul St. Mary's Hospital, College of Medicine, The Catholic University of Korea, Seoul 06591, Republic of Korea*

Jong-Won Rhie − *Department of Biomedicine and Health Sciences, College of Medicine, The Catholic University of Korea, Seoul 03083, Republic of Korea; Department of Plastic and Reconstructive Surgery, Seoul St. Mary's Hospital, College of Medicine, The Catholic University of Korea, Seoul 06591, Republic of Korea*

Tae-Suk Suh − *Department of Biomedical Engineering, College of Medicine, Catholic University of Korea, Seoul 03083, Republic of Korea*

Kyung-Don Lee − *Institute for Advanced Engineering, Yongin-si 17180, Republic of Korea*

Complete contact information is available at: https://pubs.acs.org/10.1021/acsomega.1c06974

Funding

This work was supported by National Research Foundation of Korea (NRF) grants funded by the Korean government (MSIT) [grant numbers 2017M3A9E2093907 and 2020R1A2C1012838].

Notes

The authors declare no competing financial interest.

■ ACKNOWLEDGMENTS

SEM microstructural examinations were performed at the Korea Basic Science Institute, Seoul Center.

■ ABBREVIATIONS

SEM, scanning electron microscopy; dECM, decellularized extracellular matrix; CT, X-ray computed tomography; UTM, universal testing machine; ADSCs, adipose-derived stem cells; SLS, selective laser sintering

■ REFERENCES

(1) Chu, C. F. L.; Lu, A.; Liszkowski, M.; Sipehia, R. Enhanced growth of animal and human endothelial cells on biodegradable polymers. *Biochim. Biophys. Acta (BBA) - General Subjects.* **1999**, *1472*, 479−485.
(2) Griffith, L. G.; Naughton, G. Tissue engineering–current challenges and expanding opportunities. *Science* **2002**, *295*, 1009−1014.
(3) Hench, L. L. Biomaterials: a forecast for the future. *Biomaterials.* **1998**, *19*, 1419−1423.
(4) Bigi, A.; Boanini, E.; Rubini, K. Hydroxyapatite gels and nanocrystals prepared through a sol-gel process. *J. Solid State Chem.* **2004**, *177*, 3092−3098.
(5) Hench, L. L. Bioactive ceramics: theory and clinical applications. *Bioceramics* **1994**, 3−14.
(6) Chen, Z.; Li, Z.; Li, J.; Liu, C.; Lao, C.; Fu, Y.; Liu, C.; Li, Y.; Wang, P.; He, Y. 3-D printing of ceramics: a review. *J. Eur. Ceram* **2019**, *39*, 661−687.
(7) Wang, X.; Xu, S.; Zhou, S.; Xu, W.; Leary, M.; Choong, P.; Qian, M.; Brandt, M.; Xie, Y. M. Topological design and additive manufacturing of porous metals for bone scaffolds and orthopaedic implants: A review. *Biomaterials* **2016**, *83*, 127−141.
(8) Spoerke, E. D.; Murray, N. G.; Li, H.; Brinson, L. C.; Dunand, D. C.; Stupp, S. I. A bioactive titanium foam scaffold for bone repair. *Acta Biomater.* **2005**, *1*, 523−533.
(9) Cook, S. D.; Thomas, K. A.; Delton, J. E.; Volkman, T. K.; Whitecloud, T. S.; Key, J. F. Hydroxylapatite coating of porous implants improves bone ingrowth and interface attachment strength. *J. Biomed. Mater. Res.* **1992**, *26*, 989−1001.
(10) Long, M.; Rack, H. J. Titanium alloys in total joint replacement—a materials science perspective. *Biomaterials* **1998**, *19*, 1621−1639.
(11) Wen, C.; Mabuchi, M.; Yamada, Y.; Shimojima, K.; Chino, Y.; Asahina, T. Processing of biocompatible porous Ti and Mg. *Scripta. Mater.* **2001**, *45*, 1147−1153.
(12) Suroso, I. Analysis of micro structure of result casting on drum aluminium music with metal molding. *J. Phys. Conf. Ser.* **2019**, *1175*, 012001.
(13) Liu, F. H.; Lee, R. T.; Lin, W. H.; Liao, Y. S. Selective laser sintering of bio-metal scaffold. *Procedia CIRP* **2013**, *5*, 83−87.
(14) Caeiro, J.R.; Gonzalez, P.; Guede, D. Biomechanics and bone (& II): trials in different hierarchical levels of bone and alternative tools for the determination of bone strength. *Rev. Osteoporos. Metab. Miner.* **2013**, *5*, 99−108.
(15) Ridzwan, M. I. Z.; Shuib, S.; Hassan, A. Y.; Shokri, A. A.; Ibrahim, M. N. M. Problem of stress shielding and improvement to the hip implant designs: a review. *J. Med. Sci.* **2007**, *7*, 460−467.
(16) Nagels, J.; Stokdijk, M.; Rozing, P. M. Stress shielding and bone resorption in shoulder arthroplasty. *J. Shoulder Elb. Surg.* **2003**, *12*, 35−39.
(17) Fouda, N.; Mostafa, R.; Saker, A. Numerical study of stress shielding reduction at fractured bone using metallic and composite bone-plate models. *Ain Shams Eng. J.* **2019**, *10*, 481−488.
(18) Pilliar, R. M. Porous-surfaced metallic implants for orthopedic applications. *J. Biomed. Mater. Res.* **1987**, *21*, 1−33.
(19) Woodard, J. R.; Hilldore, A. J.; Lan, S. K.; Park, C.J.; Morgan, A. W.; Eurell, J. A. C.; Clark, S. G.; Wheeler, M. B.; Jamison, R. D.; Wagoner Johnson, A. J. The mechanical properties and osteoconductivity of hydroxyapatite bone scaffolds with multi-scale porosity. *Biomaterials* **2007**, *28*, 45−54.
(20) Fujibayashi, S.; Neo, M.; Kim, H. M.; Kokubo, T.; Nakamura, T. Osteoinduction of porous bioactive titanium metal. *Biomaterials* **2004**, *25*, 443−450.
(21) Sumner, D. R.; Turner, T. M.; Urban, R. M.; Galante, J. O. Remodeling and ingrowth of bone at two years in a canine cementless total hip-arthroplasty model. *J. Bone Jt. Surg.* **1992**, *74*, 239−250.
(22) Asaoka, K.; Kuwayama, N.; Okuno, O.; Miura, I. Mechanical properties and biomechanical compatibility of porous titanium for dental implants. *J. Biomed. Mater. Res.* **1985**, *19*, 699−713.
(23) Chang, B. S.; Lee, C. K.; Hong, K. S.; Youn, H. J.; Ryu, H. S.; Chung, S. S.; Park, K. W. Osteoconduction at porous hydroxyapatite with various pore configurations. *BioMaterials* **2000**, *21*, 1291.
(24) Cheng, A.; Schwartz, Z.; Kahn, A.; Li, X.; Shao, Z.; Sun, M.; Ao, Y.; Boyan, B. D.; Chen, H. Advances in porous scaffold design for bone and cartilage tissue engineering and regeneration. *Tissue Eng. Part B Rev.* **2019**, *25*, 14−29.
(25) Michailidis, N.; Stergioudi, F. Establishment of process parameters for producing Al-foam by dissolution and powder sintering method. *Materials & Design* **2011**, *32*, 1559−1564.
(26) Baumgartner, H. R.; Steiger, R. A. Sintering and properties of titanium diboride made from powder synthesized in a plasma-arc heater. *J. Am. Ceram. Soc.* **1984**, *67*, 207−212.
(27) Martin, C. L.; Schneider, L. C. R.; Olmos, L.; Bouvard, D. Discrete element modeling of metallic powder sintering. *Scr. Mater.* **2006**, *55*, 425−428.
(28) Fischer, P.; Romano, V.; Weber, H.P.; Karapatis, N.P.; Boillat, E.; Glardon, R. Sintering of commercially pure titanium powder with a Nd:YAG laser source. *Acta Mater.* **2003**, *51*, 1651−1662.
(29) Hoshiba, T.; Lu, H.; Kawazoe, N.; Chen, G. Decellularized matrices for tissue engineering. *Expert Opin. Biol. Ther.* **2010**, *10*, 1717−1728.
(30) Kim, B. S.; Das, S.; Jang, J.; Cho, D.-W. Decellularized Extracellular Matrix-based Bioinks for Engineering Tissue- and Organ-specific Microenvironments. *Chem. Rev.* **2020**, *120* (19), 10608−10661.
(31) Lee, J. W.; Kang, K. S.; Lee, S. H.; Kim, J. Y.; Lee, B. K.; Cho, D. W. Bone regeneration using a microstereolithography-produced customized poly(propylene fumarate)/diethyl fumarate photopolymer 3D scaffold incorporating BMP-2 loaded PLGA microspheres. *Biomaterials* **2011**, *32*, 744−752.
(32) Laval-Jeantet, A.-M.; Bergot, C.; Carroll, R.; Garcia-Schaefer, F. Cortical bone senescence and mineral bone density of the humerus. *Calcif. Tissue Int.* **1983**, *35*, 268−272.
(33) Rho, J.-Y.; Kuhn-Spearing, L.; Zioupos, P. Mechanical properties and the hierarchical structure of bone. *Med. Eng. Phys.* **1998**, *20*, 92−102.
(34) Chang, B. S.; Lee, C. K.; Hong, K. S.; Youn, H. J.; Ryu, H. S.; Chung, S. S.; Park, K. W. Osteoconduction at porous hydroxyapatite with various pore configurations. *Biomaterials* **2000**, *21*, 1291.
(35) Lien, S. M.; Ko, L. Y.; Huang, T. J. Effect of pore size on ECM secretion and cell growth in gelatin scaffold for articular cartilage tissue engineering. *Acta Biomater.* **2009**, *5*, 670−679.
(36) Das, S.; Pati, F.; Choi, Y. J.; Rijal, G.; Shim, J. H.; Kim, S. W.; Ray, A. R.; Cho, D. W.; Ghosh, S. Bioprintable, cell-laden silk fibroin-gelatin hydrogel supporting multilineage differentiation of stem cells for fabrication of three-dimensional tissue construct. *Acta Biomater.* **2015**, *11*, 233−246.
(37) Pattabhi, S. R.; Martinez, J. S.; Keller, T. C. S. Decellularized ECM effects on human mesenchymal stem cell stemness and differentiation. *Differentiation* **2014**, *88*, 131−143.
(38) Hu, J.; Feng, K.; Liu, X.; Ma, P. X. Chondrogenic and osteogenic differentiations of human bone marrow-derived mesen-

https://doi.org/10.1021/acsomega.1c06974
ACS Omega 2022, 7, 10340−10346

chymal stem cells on a nanofibrous scaffold with designed pore network. *Biomaterials* **2009**, *30*, 5061−5067.
(39) Lee, M.; Chen, T. T.; Iruela-Arispe, M. L.; Wu, B. M.; Dunn, J. C. Modulation of protein delivery from modular polymer scaffolds. *Biomaterials* **2007**, *28*, 1862−1870.
(40) Lu, L.; Mikos, A. G. The importance of new processing techniques in tissue engineering. *MRS Bull.* **1996**, *21*, 28−32.

https://doi.org/10.1021/acsomega.1c06974
ACS Omega 2022, 7, 10340−10346